Maritime Anomaly Detection in a Real-World Scenario: *Ever Given* Grounding in the Suez Canal

Nicola Forti, Enrica d'Afflisio, Paolo Braca, *Senior Member, IEEE*, Leonardo M. Millefiori, *Member, IEEE*, Peter Willett, *Fellow, IEEE*, and Sandro Carniel

***Abstract*— In this paper we present how automatic maritime anomaly detection tools can be successfully applied in real-world situations such as the major event of the container vessel *Ever Given*, which grounded in the Suez Canal on March 23rd 2021. The anomaly detector is designed to process the available sequence of Automatic Identification System (AIS) reports, information from ground-based or satellite radar systems if available, and contextual information defining the expected nominal behavior of navigation. A statistical hypothesis testing procedure is sequentially run to decide whether or not a deviation from the nominal behavior happened within a specific time period, for instance two consecutive data points. We show, based on the recorded AIS data from the *Ever Given*, that the proposed detector could have been triggered and alerted to anomalous behavior fully 19 minutes before the grounding.**

***Index Terms*— Maritime anomaly detection, automatic identification system, *Ever Given* grounding, maritime surveillance, Ornstein-Uhlenbeck process, statistical hypothesis testing.**

I. Introduction

ON MARCH 23rd 2021, at 05:40 UTC, one of the world's biggest container vessels operated by Evergreen Marine Corp., the 400 m (1300 ft) *Ever Given*, was navigating northbound through the Suez Canal on its way to Rotterdam during a dust storm with wind speeds reaching 40 kn, when it became stuck in a 300 m wide channel at coordinates 30.01761°N, 32.58018°E (see Figs. 1 and 2). According to the Suez Canal Authority (SCA), the ship lost its ability to steer amid high winds and a dust storm, causing it to run aground diagonally and become wedged with its bow in one bank, and its stern nearly touching the other. The cause of the grounding is still unknown. While initial investigations exclude any mechanical or engine failure and strong winds during a dust storm are widely seen as a major factor, human and technical errors cannot be ruled out [1].

Based on the vessel tracking data available from Automatic Identification System (AIS) receivers, the maritime anomaly detector [2], [3] revealed a statistical gap between the actual and the nominal dynamic behavior expected within the canal. As is well-known, there was adverse weather and the ship lost control: it deviated in its course and collided with the bank, becoming wedged into the side of the canal (see Figs. 1 and 2).

Manuscript received 28 May 2021; revised 23 September 2021; accepted 20 October 2021. Date of publication 9 November 2021; date of current version 9 August 2022. This work was supported by the North Atlantic Treaty Organization (NATO) Allied Command Transformation (ACT) through the Project "Data Knowledge Operational Effectiveness" (DKOE). The Associate Editor for this article was Q. Ye. *(Corresponding author: Paolo Braca.)*

Nicola Forti, Enrica d'Afflisio, Paolo Braca, Leonardo M. Millefiori, and Sandro Carniel are with the NATO Science and Technology Organization (STO) Centre for Maritime Research and Experimentation (CMRE), 19126 La Spezia, Italy (e-mail: nicola.forti@cmre.nato.int; enrica.d'afflisio@cmre.nato.int; paolo.braca@cmre.nato.int; leonardo.millefiori@cmre.nato.int; sandro.carniel@cmre.nato.int).

Peter Willett is with the Department of Electrical and Computer Engineering, University of Connecticut, Storrs, CT 06269 USA (e-mail: peter.willett@uconn.edu).

Digital Object Identifier 10.1109/TITS.2021.3123890

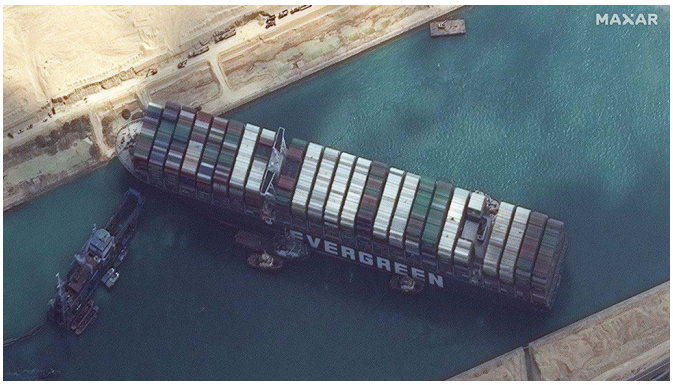

Fig. 1. A high-resolution satellite view (captured on March 25th 2021) of the *Ever Given* container ship, which grounded in the Suez Canal on March 23rd 2021. Credit: Satellite image © 2021 Maxar Technologies.

The *Ever Given* grounding had immediate consequences, resulting in the complete blockage of the Suez Canal, extensive "traffic jams" of more than 360 ships (see Fig. 2), and disruptions in the maritime global trade for six days. A similar disruption, but less intensive, was observed at global level during the first half of 2020 because of the COVID-19 pandemic, see details in [4]. As one of the world's busiest trade routes, representing nearly 12% globally, this blockage of the Suez Canal had a significant negative impact on trade between Europe and Asia [5]. It has been estimated that $9.6 billion worth of trade was held up each day as a result of the stranded ship, causing supply chain disruptions all over the world. On March 29th, at 13:04 UTC, the ship was finally freed and started moving towards the Great Bitter Lake for technical inspection, while traffic completely resumed in the canal at 17:00 UTC. A crucial assistance in the freeing of the *Ever Given* from the Suez Canal was played by an unusual full moon, which boosted a spring or "king" tide, helping the tugs refloat the ship [6].

The *Ever Given* incident illuminates the critical role of maritime surveillance on a global scale [7], [8], and automatic systems for maritime anomaly detection [2], [3], [9]–[23] based on data collected from Terrestrial and Satellite AIS (T-AIS, S-AIS), Long Range Identification and Tracking (LRIT), Vessel Monitoring System (VMS), and Earth Observation (EO) satellites, providing early warning and alert triggering to avoid issues of navigational safety such as accidents and collisions, and help to identify suspicious activities to increase security and border protection (see further details in [7], [8], [24]). Additional use cases where automatic anomaly detection systems can be beneficial in the maritime domain include detection and early warnings for vessels posing potential risks, e.g., entering forbidden areas, drifting and deviating from usual routes, and rendezvous at sea, or for vessels involved in illegal activities, e.g., drug smuggling, breaking embargoes, approaching shores to transfer goods or persons,

Fig. 2. Two views from Europe's Sentinel 1 radar observation mission show nearly 200 ships gathered on March 25th 2021 waiting for passage through the North (bottom left) and South (bottom right) entrances of the Suez Canal. The COSMO-SkyMed radar image above shows the *Ever Given* still stranded on March 25th. Credits: Copernicus Sentinel 1 data, © ESA, CC BY-SA 3.0 IGO; COSMO-SkyMed image © ASI, processed and distributed by e-GEOS.

or prohibited fishing activities such as transshipment of illegal catch (see a detailed discussion in [9]).

According to the European Maritime Safety Agency (EMSA), over the period 2014–2019 the total number of reported marine incidents was 19418, involving a total number of 21392 ships and causing 496 fatalities, mainly occurring during collisions [25]. Recent examples of major real-world accidents that shed light on the key role of maritime surveillance data for safety and security at sea include fatal crashes involving commercial and navy ships such as the USS Fitzgerald [26], and the USS John S. McCain [27], the collision between the container ship Delphis Gdansk and the cargo ship BBC Neptune in the Great Belt Strait [28], the collision between the container vessel ANL Wyongand and the gas carrier King Arthur investigated by the UK Marine Accident Investigation Branch (MAIB) [29]. An account of the transshipment of illegal sharks around the Galápagos marine reserve is available in [30]. With anomaly detection systems that provide an enhanced maritime situational picture in real or near real time, these situations can be automatically detected, alerting operators by means of, e.g., graphical user interface, e-mail, or warnings sent through the user's national system.

Nowadays, over half a million vessels use AIS to transmit their location, which is collected by a network of receivers deployed in over 140 countries and transferred for display and vessel tracking through platforms such as MarineTraffic, that has 40 million users annually alone [31]. As the AIS network of receivers grows and its technology develops from a simple navigational and situational awareness tool for safety at sea to the backbone of a global ship tracking network, AIS data is able to provide ever-more accurate and valuable information to track the position of ships anywhere in open waters or sea passageways in near real time. Present-day AIS has some limitations, e.g. it can be subject to intentional deactivation during stealthy deviations of vessels, or to malicious reporting of false information, i.e. "spoofing" [9], and message collisions in high-density traffic areas. Recent advances in maritime radio technology have given rise to the development of the VHF Data Exchange System (VDES) [32], which provides higher data rates and enables both full duplex and encrypted communications. Large volumes of streams of AIS messages were recently processed to visualize ship routes and traffic density maps [33], identify global patterns of transshipment behavior [34], analyze the effects of COVID-19 on global maritime mobility [4], and to train deep learning networks for long-term prediction of vessel trajectories [35]. This information is also fundamental to enable advanced anomaly detection systems for the maritime domain to make decisions based on near real-time data that can help avoid incidents such as the grounding of the *Ever Given*.

Recent advances in maritime anomaly detection based on an innovative statistical representation of vessel tracking data available from surveillance systems such as AIS open up the possibility to reveal vessel deviations from standard navigational routes as well as "dark" anomalous behaviors in the presence of data gaps (due to, e.g., AIS disablements or limited coverage). In particular, the anomaly detector proposed in [2], which models the dynamics of vessels through the Ornstein-Uhlenbeck (OU) stochastic process and exploits contextual information to define the nominal behavior at sea, runs a hypothesis testing procedure to detect anomalous deviations within a given time window based on the available vessel contacts. Recent work on anomaly detection strategies building on the OU model for maritime data can be found in [2], [3], [9]–[13], [35].

In this paper, we show how these automatic anomaly detection tools could have been successfully applied to the real-world maritime scenario of the *Ever Given* using the available sequence of AIS records, and contextual information defining the expected nominal behavior of navigation. An anomaly detection strategy based on statistical hypothesis testing, as described in Section II, is sequentially run between two consecutive AIS records to decide whether or not a deviation from the nominal behavior happened within that specific time period. Our results in Section III reveal an anomalous behavior of the ship, detected 19 minutes before the grounding, which could have helped avoid the accident that caused such a negative impact on maritime traffic and global trade.

Alternative methods that could be applied to the scenario under consideration include [14]–[23]. However, to the best of our knowledge, this is the first time that an automatic anomaly detection procedure is applied to the real-world data of the *Ever Given* grounding.

II. Maritime Anomaly Detection Based on the OU Stochastic Model

Let us consider a ship of interest which is sailing as a moving point object in a two-dimensional space, with a kinematic state at time $t \in \mathbb{R}_0^+$ denoted by $\boldsymbol{s}(t) = [\boldsymbol{x}(t), \dot{\boldsymbol{x}}(t)]^T$, where $\boldsymbol{x}(t)$ and $\dot{\boldsymbol{x}}(t)$ represent the ship position and velocity, respectively, in a two-dimensional Cartesian reference system

$$\boldsymbol{x}(t) = [x(t),\ y(t)]\,,\ \dot{\boldsymbol{x}}(t) = [\dot{x}(t),\ \dot{y}(t)]\,, \tag{1}$$

resulting from the projection of the geographic coordinates reported by the available (e.g., AIS, radar) contacts of the ship. Given a specific time window, for instance between two consecutive measurements of the ship, the goal is to decide whether or not a deviation from nominal behavior (i.e., an anomalous behavior) happened in that specific time interval, relying upon a suitable motion model for the vessel of interest, a measurement model for the received contacts, and

any contextual information available to define the nominal behavior. The specifics of the aforementioned elements are described in the following subsections.

The OU motion model [36] has been recently proposed as an accurate representation of the time evolution of vessel kinematic states, which differs from conventional nearly-constant velocity models by assuming the velocity is an OU mean-reverting stochastic process, whose variance stays bounded around a long-run mean value, instead of tending to diverge with time. In this work, we assume that the vessel moves following a piecewise OU model [37], which is an extension of the single OU model for non-maneuvering vessels [36] to the case of navigation along multiple waypoints, by assuming that the long-run mean velocity of the vessel is a piecewise-constant function of time, taking values from a sequence $\boldsymbol{v}_1, \ldots, \boldsymbol{v}_N$. In this case, along the N navigational legs, the long-run mean velocity of the process is constant and the instantaneous velocity of the vessel follows an OU process; conversely, during the maneuver from one leg to another, the long-run mean velocity parameter will change its value. Under this assumption, the OU motion model in a generic navigational leg $n = 1, \ldots, N$ describing the vessel state $\boldsymbol{s}_n = \boldsymbol{s}(t_n)$, given the state at the previous time t_{n-1}, takes the following form

$$\boldsymbol{s}_n = \boldsymbol{\Phi}(\Delta_n, \boldsymbol{\gamma})\boldsymbol{s}_{n-1} + \boldsymbol{\Psi}(\Delta_n, \boldsymbol{\gamma})\boldsymbol{v}_n + \boldsymbol{\omega}_n, \tag{2}$$

where: $\boldsymbol{v}_n = \left[v_{n_x}, v_{n_y}\right]^T$ is the long-run mean velocity in the time interval $\Delta_n = t_n - t_{n-1}$; $\boldsymbol{\gamma} = [\gamma_x, \gamma_y]^T$ is the reversion rate, i.e. the rate at which the vessel velocity tends back to its long-run mean; $\boldsymbol{\omega}_n = \boldsymbol{\omega}(t_n)$ is a zero-mean Gaussian random variable with covariance $\mathbf{C}(\Delta_n, \boldsymbol{\gamma}, \boldsymbol{\sigma})$; $\boldsymbol{\Phi}(\Delta_n, \boldsymbol{\gamma})$ and $\boldsymbol{\Psi}(\Delta_n, \boldsymbol{\gamma})$ are the state transition, and, respectively, the control input matrix, all defined in [36]. In summary, we assume that in each considered time window the vessel moves according to the piecewise OU model (2) specified by a sequence of long-run mean velocities $\boldsymbol{v}_n, n = 1, \ldots, N$, along with other two parameters: the reversion rate $\boldsymbol{\gamma}$, and the process noise standard deviation $\boldsymbol{\sigma} = [\sigma_x, \sigma_y]^T$. Note that, the vessel state at time t_N, given the target states at the previous $N-1$ times, can be written as

$$\boldsymbol{s}_N = \boldsymbol{\Phi}(T)\boldsymbol{s}_0 + \boldsymbol{\Psi}(\Delta_N)\boldsymbol{v}_N + \boldsymbol{\omega}_N + \sum_{n=1}^{N-1}\left[\prod_{i=n+1}^{N}\boldsymbol{\Phi}(\Delta_i)\right]\left[\boldsymbol{\Psi}(\Delta_n)\boldsymbol{v}_n + \boldsymbol{\omega}_n\right], \tag{3}$$

where $T = \sum_{n=1}^{N}\Delta_n$. In (3) we omitted $\boldsymbol{\gamma}$ for clarity, and exploited the property of the state transition matrix by which $\boldsymbol{\Phi}(\Delta_1)\boldsymbol{\Phi}(\Delta_2)\ldots\boldsymbol{\Phi}(\Delta_n) = \boldsymbol{\Phi}(\Delta_1 + \Delta_2 + \ldots + \Delta_n)$, $\forall n = 1, \ldots, N$, (see [2]).

A. Measurement Model

Let us assume there are $K+1$ measurements available (e.g., from AIS, radar) within a specific time window of length T. The k-th measurement is available at time $T_k = \frac{p_k}{N}T$, where $p_k \in [0, N]$ is a fraction of the interval $[0, N]$ representing the time location of the contact with respect to the N piecewise OU velocities. Then, each measurement can be modeled as

$$\boldsymbol{m}_k = \boldsymbol{s}(T_k) + \boldsymbol{n}_k, \qquad k = 0, \ldots, K \tag{4}$$

where $\boldsymbol{s}(T_k)$ can be obtained from (3), and the measurement noise $\boldsymbol{n}_k$ is assumed to be independent and identically distributed according to a zero-mean Gaussian with covariance matrix $\mathbf{C}_{\boldsymbol{n}_k}$.

In order to avoid the dependency of $\boldsymbol{m}_k$ on the OU initial state $\boldsymbol{s}_0$ through $\boldsymbol{s}(T_k)$, it is convenient to consider the sequence of data $\boldsymbol{y} = [\boldsymbol{y}_1^T, \ldots, \boldsymbol{y}_K^T]^T$, obtained from the measurement vector (4) as

$$\boldsymbol{y}_k = \boldsymbol{m}_k - \boldsymbol{\Phi}(T_k)\boldsymbol{m}_0, \tag{5}$$

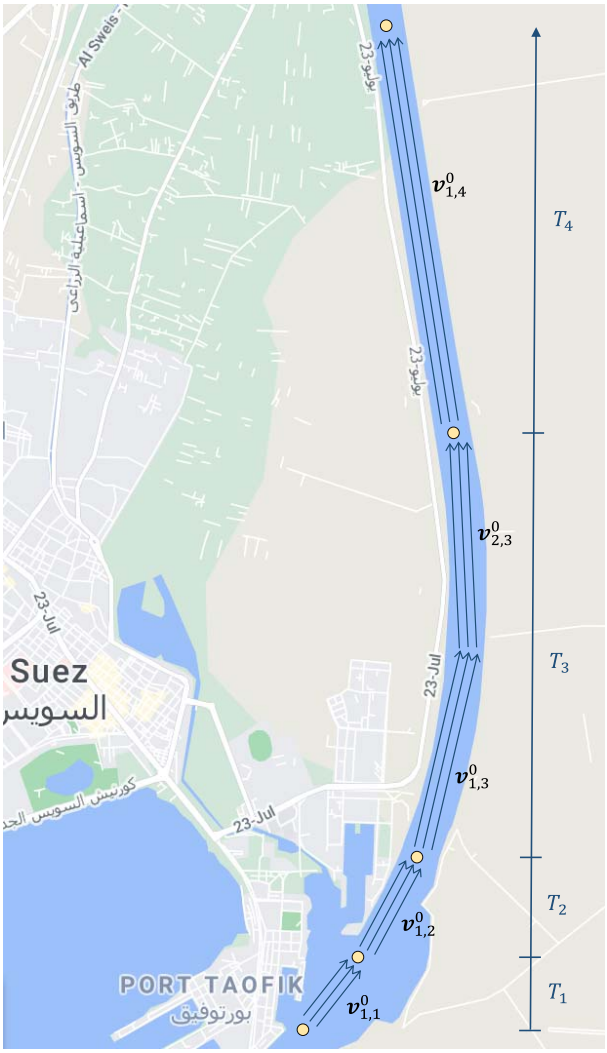

Fig. 3. Sequence of OU velocities and time intervals characterizing the nominal dynamic behavior of the *Ever Given* inside the Suez Canal given the available sequence of AIS contacts.

where $\boldsymbol{m}_0$ is the first contact available denoting the initial point of the considered time window.

B. Anomaly Detection Strategy

The considered anomaly detection problem amounts to determining whether or not the vessel moving according to a piecewise OU model has been following the nominal dynamic behavior in a specific time window $t_0 < t_1 < \ldots < t_N = T$. The inference should be based on the statistical gap between the actual and the nominal sequence of OU long-run mean velocities, i.e. between the $2N$-dimensional column vectors $\boldsymbol{v} \triangleq \text{col}\{\boldsymbol{v}_n\}_{n=1}^N$ and, respectively, $\boldsymbol{v}_0 \triangleq \text{col}\{\boldsymbol{v}_n^0\}_{n=1}^N$, with $\boldsymbol{v}_n^0$ denoting the n-th nominal long-run mean velocity along x and y coordinates. As shown in [2], the problem can be traced back to the following Gaussian composite hypothesis testing formulation designed to identify changes in the OU long-run velocity parameter:

$$\begin{cases} H_0: \ \boldsymbol{y} \sim \mathcal{N}\left(\boldsymbol{\mu}_0, \mathbf{C}_{\boldsymbol{y}}\right) \\ H_1: \ \boldsymbol{y} \sim \mathcal{N}\left(\boldsymbol{\mu}, \mathbf{C}_{\boldsymbol{y}}\right) \end{cases} \tag{6}$$

where the null hypothesis, H_0, states that the vessel navigates according to the nominal condition, and, alternatively, H_1 states that

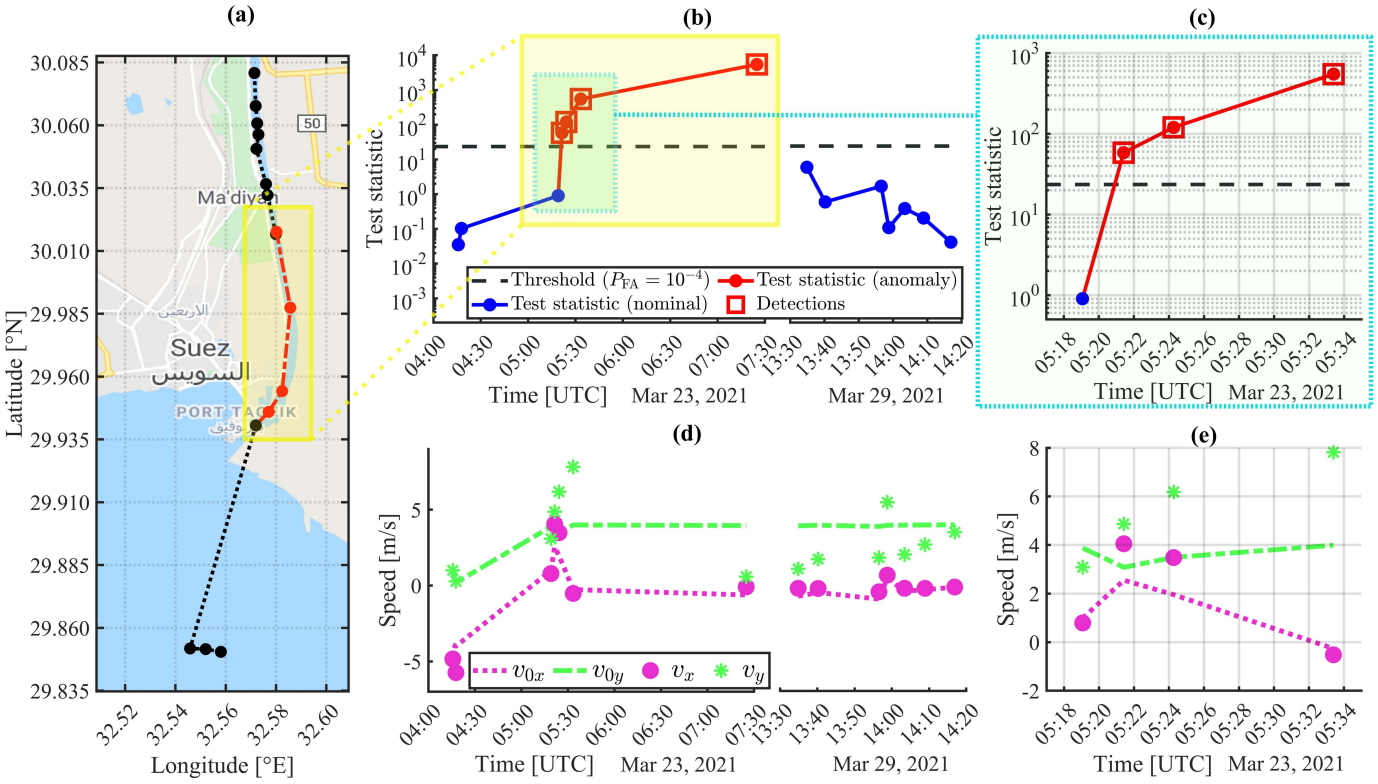

Fig. 4. (a) *Ever Given* trajectory reported by T-AIS and S-AIS from 23-03-21 to 29-03-21. Please note that the AIS trajectory is obtained by simply connecting the available contacts (circles) with a dotted line. (b) Test statistic of the anomaly detector over the period pre- and post-grounding of the *Ever Given*. (c) Close-up of the evolution of the anomaly test statistic during the navigation of the ship inside the Suez Canal until the time of the last AIS contact before grounding (i.e., from 05:19 to 05:33 UTC, 23-03-21). (d) Velocity components of the ship along the x- and y-axis over the period pre- and post-grounding. (e) Close-up of the velocity components during the navigation of the ship inside the canal before grounding.

the vessel moves away from the nominal condition. The mean vectors in (6) are given by

$$\boldsymbol{\mu}_0 = \mathbf{H}\,\boldsymbol{v}_0, \qquad \boldsymbol{\mu} = \mathbf{H}\,\boldsymbol{v}, \tag{7}$$

where $\mathbf{H} \in \mathbb{R}^{4K\times 2N}$ is the model matrix defined in [2], assumed known, which depends on the state transition and control input matrices associated to the k-th contact. The covariance matrix $\mathbf{C}_{\boldsymbol{y}}$ in (6) $\forall i, j = 1, \ldots, K$ is given by (see [2], Appendix C)

$$\mathbf{C}_{ij} = \begin{cases} \mathbf{C}(T_i) + \mathbf{C}_{\boldsymbol{n}_i} + \boldsymbol{\Phi}(T_i)\mathbf{C}_{\boldsymbol{n}_0}\boldsymbol{\Phi}(T_i)^T & \text{if } i = j \\ \mathbf{C}(T_i)\boldsymbol{\Phi}(T_j - T_i)^T + \boldsymbol{\Phi}(T_i)\mathbf{C}_{\boldsymbol{n}_0}\boldsymbol{\Phi}(T_j)^T & \text{if } i < j \end{cases}$$

and $\mathbf{C}_{ji} = \mathbf{C}_{ij}^T$.

The anomaly detection strategy for the hypothesis testing problem (6) is based on the Generalized Likelihood Ratio Test (G-LRT) approach [38], and takes the form [2]

$$(\widehat{\boldsymbol{v}} - \boldsymbol{v}_0)^T\,\mathbf{H}^T\mathbf{C}_{\boldsymbol{y}}^{-1}\mathbf{H}\,(\widehat{\boldsymbol{v}} - \boldsymbol{v}_0) \underset{H_0}{\overset{H_1}{\gtrless}} \tau, \tag{8}$$

where τ is the test threshold, and $\widehat{\boldsymbol{v}}$ denotes the Maximum Likelihood (ML) estimate for the parameter $\boldsymbol{v}$, given by

$$\widehat{\boldsymbol{v}} = \left(\mathbf{H}^T\mathbf{C}_{\boldsymbol{y}}^{-1}\mathbf{H}\right)^{-1}\mathbf{H}^T\mathbf{C}_{\boldsymbol{y}}^{-1}\boldsymbol{y}. \tag{9}$$

The test performance is defined in terms of false alarm probability P_{FA}, i.e., the probability that the test statistic exceeds the threshold under H_0, and detection probability P_{D}, i.e., the probability that the test statistic exceeds the threshold under H_1. As shown in [2], the test statistics under the two hypotheses H_0 and H_1 are characterized, respectively, by a central and a non-central Chi-squared distribution, both with $d = 2N$ degrees of freedom, corresponding to the size of the known parameter $\boldsymbol{v}_0$. Therefore, the detection performance can be specified in terms of the following quantities:

$$P_{\text{FA}} = Q_{\chi_d^2}(\tau), \qquad P_{\text{D}} = Q_{\chi_d'^2(\lambda)}(\tau), \tag{10}$$

where $Q_{\chi_d^2}$ and $Q_{\chi_d'^2(\lambda)}$ are the right tail probabilities of the central and non-central Chi-squared distributions, respectively, and λ is the non-centrality parameter

$$\lambda = (\boldsymbol{v} - \boldsymbol{v}_0)^T\,\mathbf{C}_{\boldsymbol{y}}^{-1}\,(\boldsymbol{v} - \boldsymbol{v}_0)\,. \tag{11}$$

C. Configuration of Model Parameters and Nominal Behavior

A configuration of the process parameters of the OU dynamic model introduced in the previous subsections, including the nominal velocities characterizing the expected behavior of the vessel, must be set in order to apply the GLRT (8) for anomaly detection to the available data set. The statistical hypothesis testing is sequentially run between two consecutive AIS data points to decide whether or not a deviation from the nominal behavior happened within that interval. In each time window of length T_j, $j = 1, 2, \ldots, M$, the vessel is assumed to move according to a piecewise OU model specified by a sequence of OU processes with unknown long-run mean velocities, or equivalently, a single OU process with long-run mean velocity that is a piecewise-constant function of time. Under H_0, the vessel is expected to move along a planned trajectory according to a piecewise OU model characterized by a sequence $\boldsymbol{v}_{0,j} = \text{col}\{\boldsymbol{v}_{n,j}^0\}_{n=1}^{N_j^0}$ of nominal velocities, identifying an N_j^0-section nominal path within the j-th time frame (see Fig. 3). Alternatively, under H_1, the vessel

is assumed to move away from the nominal condition by following a sequence $\boldsymbol{v}_j = \text{col}\{\boldsymbol{v}_{n,j}\}_{n=1}^{N_j}$ of N_j velocities, where, in general, $N_j \neq N_j^0$.

Typically, nominal behavior of ships can be defined based on contextual information such as historical data, trajectory plans, and rules of navigation such as the International Regulations for Preventing Collisions at Sea (COLREGs) published by the International Maritime Organization (IMO), to be followed by vessels at sea. In this case, given the characteristics of the navigation area, the expected nominal behavior of the *Ever Given* inside the canal as shown in Fig. 3 was defined based on i) the trajectory path to be followed considering its geographical constraints, and ii) speed of transit limits put in place by the SCA [39]. In particular, we considered a constant nominal speed $v_0 = 4$ m/s, below the limit of 4.44 m/s (16 km/h) for ordinary vessels, and consistent with an average transit time of 14 hours to navigate a canal with a length of 193.3 km. Note that the uncertainty about the nominal speed v_0 is taken into account through a suitable choice of the nominal OU process noise standard deviation. Then, the x and y components of the nominal velocity vectors $\boldsymbol{v}_{n,j}^0$, $n = 1, \ldots, N_j^0$, are obtained using the nominal speed and course angle computed for each section of the planned trajectory path as shown in Fig. 3 for the trajectory segment inside the canal and before grounding. The same nominal speed is applied to the entire AIS trajectory shown in Fig. 4(a).

In addition, the parameters of the underlying OU process were selected following the statistical features estimated for the cargo traffic category in [36]. However, given that this configuration of OU parameters is typically used in open-water navigation where the motion of vessels involves larger distances and longer time frames for which a steady-state behavior of the process can be assumed, for this case in the canal we have applied an adjustment factor $\alpha = 200$ to the reversion rate, to account for a shorter time scale with faster transient dynamics. The same factor was applied to the noise variance so as to keep the same ratio $\boldsymbol{\sigma}^2/\boldsymbol{\gamma}$, shown to be proportional to the asymptotic OU uncertainty [36]. In particular, we set the reversion rate and process noise level as $\bar{\boldsymbol{\gamma}} = [6.28 \times 10^{-4}, 5.63 \times 10^{-4}]$, $\bar{\boldsymbol{\sigma}} = [9.04 \times 10^{-3}, 9.17 \times 10^{-3}]$ outside the canal, and $\boldsymbol{\gamma} = \alpha\bar{\boldsymbol{\gamma}}$, $\boldsymbol{\sigma}^2 = \alpha\bar{\boldsymbol{\sigma}}^2$ inside the canal.

III. Anomaly Detection Case Study: *Ever Given* Grounding

The maritime anomaly detection strategy presented in Section II is applied to the AIS data set of the *Ever Given*, reported from 23-03-21 to 29-03-21, in order to detect an anomaly in its motion before grounding, which occurred at 05:40 UTC, 23-03-21. The AIS track of interest, shown in Fig. 4(a), spans over three time periods: the period when the ship is navigating outside the canal, the period when the ship is inside the canal until the grounding, and the period post-grounding. The first AIS contacts starting from 04:13 UTC, 23-03-21 are outside the canal when the ship starts moving on March 23rd towards the South entrance. Then, five key contacts are received and highlighted in our area of interest (AoI) in Fig. 4(a), of which four, at 05:19, 05:21, 05:24, and 05:33 UTC, respectively, are before grounding. The fifth data point in the AoI represents the first contact available (07:24 UTC) once the *Ever Given* is stranded. Then, we reported seven AIS contacts of the ship moving northbound after being finally freed on March 29th at 13:04 UTC.

The hypothesis testing procedure described in Section II is run between two consecutive AIS contacts to determine whether or not deviation occurred from the nominal behavior during that time window. The red segments in Fig. 4(a) show an anomalous behavior detected just after entrance to the canal at the second AIS contact

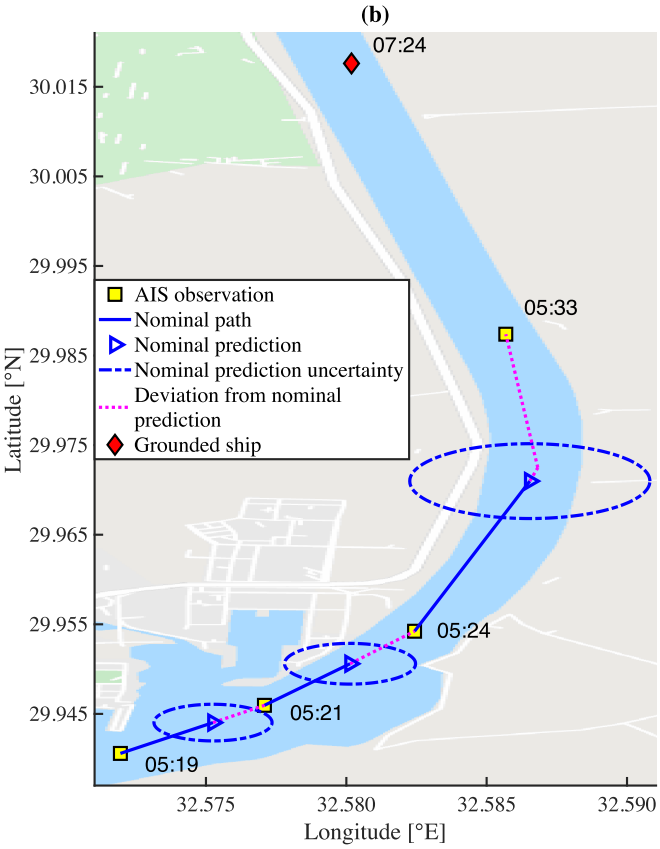

Fig. 5. Predicted nominal path of the ship (blue solid line) and predicted nominal position (blue triangle) with related uncertainty (blue ellipse) compared to the actual AIS observations (yellow squares) received inside the canal before grounding.

inside (05:21 UTC, 23-03-21), and again at two other contacts (05:24, 05:33 UTC) immediately before the grounding. The last detection of an anomaly occurred at the first AIS contact (07:24 UTC), which is after the accident. Otherwise, no anomaly is reported before sailing through the Suez Canal or after the accident. Fig. 4(b) displays the test statistic (8) of the anomaly detector over the period pre- and post-grounding, which is shown to exceed the threshold within four intervals of the AIS track with false alarm probability $P_{\text{FA}} = 10^{-4}$ corresponding to the deviation from the nominal condition. The velocity components of the ship along the x- and y-axis (longitude and latitude, respectively) are displayed for the same time period in Fig. 4(d). These components are obtained using the projections of geographical position coordinates in a two-dimensional Cartesian reference system. Fig. 4(c) shows a close-up of the evolution of decision statistic during the navigation of the ship corresponding to the four contacts inside the Suez Canal and before grounding where a deviation from the nominal behavior was detected in three time intervals. From Fig. 4(c), note that the velocity component in the x-direction (orange ○), despite constraints due to the geographical characteristics of the passage, shows a clear alteration from the nominal behavior (orange dot line) at two time points (05:21 and 05:24 UTC) where the velocity is shown to be abnormally higher than expected. This alteration of the velocity along the x direction could be an indication of swerving, that combined with the increased speed along the y direction, could have contributed to the cause of the *Ever Given*'s grounding.

An intuitive analysis on the operating principle behind the anomaly detection strategy (8) is provided in Fig. 5, where we can see

the predicted nominal behavior of the ship (blue solid line), and the predicted position (blue triangle) with related uncertainty (blue ellipse), corresponding to the decision test run for the three contacts inside the canal and before grounding as shown in Fig. 4(c). Each prediction in Fig. 5 is obtained through the OU dynamic model (2) or, equivalently, (3) given the nominal parameters, and the time frame between the current and last AIS observation, with the last contact as initial state. The magenta dotted lines represent the actual deviation between the nominal prediction of the ship and the observed position. Intuitively, an anomaly behavior between two observations is detected through the GLRT (8) whenever the actual position of the ship available from the AIS contact falls outside the uncertainty region associated with the predicted nominal position. In practice, this is due to the difference between the nominal and estimated OU velocity parameters within the time window of interest. This difference in velocity is evident in Fig. 4(e) for the three AIS contacts at 05:21, 05:24, and 05:33 UTC, which for this reason fall outside the predicted uncertainty region of the nominal position as shown in Fig. 5. This, in turn, makes the test statistic exceed the threshold, hence revealing three anomalies as shown in Fig. 4(c).

Based on our results derived from real-world data of the *Ever Given*, one could see how the ship traveling at a speed statistically higher than the nominal one to be adopted in the Suez Canal, would have triggered the anomaly detector 19 minutes before the grounding.

IV. Conclusion

A maritime anomaly detection strategy based on statistical hypothesis testing is applied to the real-world scenario of the *Ever Given* grounding in the Suez Canal using the sequence of AIS records available from the ship. Anomaly detection relies on three key components: i) a dynamic model for the vessel of interest, ii) a measurement model for the received contacts, iii) and contextual information defining the expected nominal behavior for safe navigation in the canal. Through our results we show how automatic processing of the aforementioned information could have detected an anomalous behavior of the ship 19 minutes before the grounding. This early detection could have potentially assisted in the safe navigation of the ship during the critical moments before the accident. This, in turn, would have potentially helped to better understand and evaluate the anomaly, and improve the decision-making process in human-computer interaction, hence emphasizing the importance of automatic anomaly detection systems in real-world maritime situations.

Acknowledgment

This paper and any results herein presented are intended for scientific dissemination only. Any views or opinions expressed in this paper do not necessarily reflect NATO's policy.

References

[1] *Who Pays for Suez Blockage Ever Given Grounding Could Spark Years of Litigation*. The Guardian. Accessed: Oct. 30, 2021. [Online]. Available: https://www.theguardian.com/business/2021/mar/30/years-of-litigation-co%uld-lie-ahead-as-insurers-eye-cost-of-ever-given-grounding

[2] E. d'Afflisio, P. Braca, L. M. Millefiori, and P. Willett, "Detecting anomalous deviations from standard maritime routes using the Ornstein–Uhlenbeck process," *IEEE Trans. Signal Process.*, vol. 66, no. 24, pp. 6474–6487, Dec. 2018.

[3] E. d'Afflisio, P. Braca, L. M. Millefiori, and P. Willett, "Maritime anomaly detection based on mean-reverting stochastic processes applied to a real-world scenario," in *Proc. 21st Int. Conf. Inf. Fusion (FUSION)*, Jul. 2018, pp. 1171–1177.

[4] L. M. Millefiori *et al.*, "COVID-19 impact on global maritime mobility," *Sci. Rep.*, vol. 11, no. 1, pp. 1–16, Dec. 2021.

[5] *A Perfect Storm for Container Shipping*. The Economist. Accessed: Oct. 30, 2021. [Online]. Available: https://www.economist.com/finance-and-economics/a-perfect-storm-for-container-shipping/21804500

[6] *How a Full Moon and a Huge Lever Helped Free Ever Given From Suez Canal*. The Guardian. Accessed: Oct. 30, 2021. [Online]. Available: https://www.theguardian.com/world/2021/mar/30/powerful-tugs-and-an-ebbing-tide-how-the-ever-given-was-freed

[7] G. Soldi *et al.*, "Space-based global maritime surveillance. Part I: Satellite technologies," *IEEE Aerosp. Electron. Syst. Mag.*, vol. 36, no. 9, pp. 8–28, Sep. 2021.

[8] G. Soldi *et al.*, "Space-based global maritime surveillance. Part II: Artificial intelligence and data fusion techniques," *IEEE Aerosp. Electron. Syst. Mag.*, vol. 36, no. 9, pp. 30–42, Sep. 2021.

[9] E. d'Afflisio, P. Braca, and P. Willett, "Malicious AIS spoofing and abnormal stealth deviations: A comprehensive statistical framework for maritime anomaly detection," *IEEE Trans. Aerosp. Electron. Syst.*, vol. 57, no. 4, pp. 2093–2108, Aug. 2021.

[10] N. Forti, L. M. Millefiori, and P. Braca, "Hybrid Bernoulli filtering for detection and tracking of anomalous path deviations," in *Proc. 21st Int. Conf. Inf. Fusion (FUSION)*, Jul. 2018, pp. 1178–1184.

[11] N. Forti, L. M. Millefiori, P. Braca, and P. Willett, "Anomaly detection and tracking based on mean–reverting processes with unknown parameters," in *Proc. IEEE Int. Conf. Acoust., Speech Signal Process. (ICASSP)*, May 2019, pp. 8449–8453.

[12] N. Forti, L. M. Millefiori, P. Braca, and P. Willett, "Random finite set tracking for anomaly detection in the presence of clutter," in *Proc. IEEE Radar Conf. (RadarConf)*, Sep. 2020, pp. 1–6.

[13] N. Forti, L. M. Millefiori, P. Braca, and P. Willett, "Bayesian filtering for dynamic anomaly detection and tracking," *IEEE Trans. Aerosp. Electron. Syst.*, to be published.

[14] B. Ristic, B. L. Scala, M. Morelande, and N. Gordon, "Statistical analysis of motion patterns in AIS data: Anomaly detection and motion prediction," in *Proc. 11th Int. Conf. Inf. Fusion*, Jun. 2008, pp. 1–7.

[15] R. O. Lane, D. A. Nevell, S. D. Hayward, and T. W. Beaney, "Maritime anomaly detection and threat assessment," in *Proc. 13th Int. Conf. Inf. Fusion*, Jul. 2010, pp. 1–8.

[16] K. Kowalska and L. Peel, "Maritime anomaly detection using Gaussian process active learning," in *Proc. 15th Int. Conf. Inf. Fusion*, Jul. 2012, pp. 1164–1171.

[17] M. Vespe, I. Visentini, K. Bryan, and P. Braca, "Unsupervised learning of maritime traffic patterns for anomaly detection," in *Proc. 9th IET Data Fusion Target Tracking Conf. (DF&TT), Algorithms Appl.*, 2012, pp. 1–6.

[18] C. Zor and J. Kittler, "Maritime anomaly detection in ferry tracks," in *Proc. IEEE Int. Conf. Acoust., Speech Signal Process. (ICASSP)*, Mar. 2017, pp. 2647–2651.

[19] B. Liu, E. N. de Souza, C. Hilliard, and S. Matwin, "Ship movement anomaly detection using specialized distance measures," in *Proc. 18th Int. Conf. Inf. Fusion*, Jul. 2015, pp. 1113–1120.

[20] D. Zissis, E. K. Xidias, and D. Lekkas, "Real-time vessel behavior prediction," *Evolving Syst.*, vol. 7, no. 1, pp. 29–40, Mar. 2016.

[21] R. Zhen, Y. Jin, Q. Hu, Z. Shao, and N. Nikitakos, "Maritime anomaly detection within coastal waters based on vessel trajectory clustering and Naïve Bayes classifier," *J. Navigat.*, vol. 70, no. 3, pp. 648–670, May 2017.

[22] L. Zhao and G. Shi, "Maritime anomaly detection using density-based clustering and recurrent neural network," *J. Navigat.*, vol. 72, no. 4, pp. 894–916, Jul. 2019.

[23] I. Kontopoulos, K. Chatzikokolakis, D. Zissis, K. Tserpes, and G. Spiliopoulos, "Real-time maritime anomaly detection: Detecting intentional AIS switch-off," *Int. J. Big Data Intell.*, vol. 7, no. 2, pp. 85–96, 2020.

[24] D. Gaglione *et al.*, "Bayesian information fusion and multitarget tracking for maritime situational awareness," *IET Radar, Sonar Navigat.*, vol. 14, no. 2, pp. 1845–1857, Nov. 2020.

[25] (2020). *Annual Overview of Marine Casualties and Incidents 2020*. EMSA, Tech. Rep. Accessed: Apr. 30, 2021. [Online]. Available: http://www.emsa.europa.eu/newsroom/latest-news/item/4266-annual-overvie%w-of-marine-casualties-and-incidents-2020.html

[26] *USS Fitzgerald Crash: Seven Navy Crew Missing Off Japan*. BBC News. Accessed: Oct. 30, 2021. [Online]. Available: https://www.bbc.com/news/world-asia-40310563

[27] *U.S. Destroyer Collides With Tanker Off Singapore; 10 Missing*. NBC News. Accessed: Oct. 30, 2021. [Online]. Available: https://www.nbcnews.com/news/world/navy-destroyer-uss-john-s-mccain-col%lides-merchant-ship-east-n794386

[28] *Freighter and Boxship Collide off Denmark*. The Maritime Executive. Accessed: Oct. 30, 2021. [Online]. Available: https://www.maritime-executive.com/article/freighter-and-boxship-collid%e-off-denmark

[29] (2020). *Collision Between Container Vessel ANL Wyong and Gas Carrier King Artur*. UK Marine Accident Investigation Branch. Accessed: May 9, 2021. [Online]. Available: https://www.gov.uk/maib-reports/collision-between-container-vessel-anl-%wyong-and-gas-carrier-king-arthur

[30] J. J. Alava *et al.*, "Massive Chinese fleet jeopardizes threatened shark species around the Galápagos marine reserve and waters off Ecuador: Implications for national and international fisheries policy," *Int. J. Fisheries Sci Res.*, vol. 1, no. 1, p. 1001, 2017.

[31] *Seven Things You Should Know About AIS*. MarineTraffic Blog. Accessed: Oct. 30, 2021. [Online]. Available: https://www.marinetraffic.com/blog/seven-things-know-ais

[32] *VHF Data Exchange System (VDES) Overview*. IALA Guideline VDES. Accessed: Oct. 30, 2021. [Online]. Available: https://www.iala-aism.org/product/vhd-data-exchange-system-vdes-overvie%w-1117

[33] M. Fiorini, A. Capata, and D. D. Bloisi, "AIS data visualization for maritime spatial planning (MSP)," *Int. J. e-Navigat. Maritime Economy*, vol. 5, pp. 45–60, Dec. 2016.

[34] N. A. Miller, A. Roan, T. Hochberg, J. Amos, and D. A. Kroodsma, "Identifying global patterns of transshipment behavior," *Frontiers Mar. Sci.*, vol. 5, p. 240, Jul. 2018.

[35] S. Capobianco, L. M. Millefiori, N. Forti, P. Braca, and P. Willett, "Deep learning methods for vessel trajectory prediction based on recurrent neural networks," *IEEE Trans. Aerosp. Electron. Syst.*, early access, Jul. 21, 2021, doi: 10.1109/TAES.2021.3096873.

[36] L. M. Millefiori, P. Braca, K. Bryan, and P. Willett, "Modeling vessel kinematics using a stochastic mean-reverting process for long-term prediction," *IEEE Trans. Aerosp. Electron. Syst.*, vol. 52, no. 5, pp. 2313–2330, Oct. 2016.

[37] P. Coscia, P. Braca, L. M. Millefiori, F. A. N. Palmieri, and P. Willett, "Multiple Ornstein–Uhlenbeck processes for maritime traffic graph representation," *IEEE Trans. Aerosp. Electron. Syst.*, vol. 54, no. 5, pp. 2158–2170, Oct. 2018.

[38] B. Porat and B. Friedlander, "Performance analysis of a class of transient detection algorithms—A unified framework," *IEEE Trans. Signal Process.*, vol. 40, no. 10, pp. 2536–2546, Oct. 1992.

[39] Suez Canal Authority, "Rules of navigation," Ismailia, Egypt, Tech. Rep., Aug. 2015. Accessed: May 6, 2021. [Online]. Available: https://www.suezcanal.gov.eg/English/Navigation/Pages/RulesOfNavigation%.aspx